International Journal of Modern Physics C
Vol. 25, No. 3 (2014) 1350095 (15 pages)

DOI: 10.1142/S0129183113500952

World Scientific
www.worldscientific.com

Complex network structure of flocks in the Vicsek Model with Vectorial Noise

Gabriel Baglietto

Instituto de Física de Líquidos y Sistemas Biológicos (CONICET, UNLP)
59 Nro 789, 1900 La Plata, Argentina
Facultad de Ingeniería (UNLP), La Plata, Argentina
Gr. Coll. Roma I, V.le Regina Elena 299, 00161 Roma, Italy
gabriel.baglietto@gmail.com

Ezequiel V. Albano

Instituto de Física de Líquidos y Sistemas Biológicos (CONICET, UNLP)
59 Nro 789, 1900 La Plata, Argentina
Departamento de Física, Facultad de Ciencias Exactas (UNLP)
La Plata, Argentina
ezequielalb@yahoo.com.ar

Julián Candia

Instituto de Física de Líquidos y Sistemas Biológicos (CONICET, UNLP)
59 Nro 789, 1900 La Plata, Argentina
Department of Physics, University of Maryland
College Park, MD 20742, USA
candia@umd.edu

Received 10 August 2013
Accepted 1 September 2013
Published 25 September 2013

In the Vicsek Model (VM), self-driven individuals try to adopt the direction of movement of their neighbors under the influence of noise, thus leading to a noise-driven order–disorder phase transition. By implementing the so-called Vectorial Noise (VN) variant of the VM (i.e. the VM-VN model), this phase transition has been shown to be discontinuous (first-order). In this paper, we perform an extensive complex network study of VM-VN flocks and show that their topology can be described as highly clustered, assortative, and nonhierarchical. We also study the behavior of the VM-VN model in the case of "frozen flocks" in which, after the flocks are formed using the full dynamics, particle displacements are suppressed (i.e. only rotations are allowed). Under this kind of restricted dynamics, we show that VM-VN flocks are unable to support the ordered phase. Therefore, we conclude that the particle displacements at every time-step in the VM-VN dynamics are a key element needed to sustain long-range ordering throughout.

Keywords: Self-propelled particle systems; collective motion; complex networks; Vicsek model.

1. Introduction

Flocking phenomena have attracted great interdisciplinary interest due to their fascinating characteristics and their ubiquity at all scales, as well as due to their complex nature. Modeling of swarming and flocking contributes to the understanding of natural phenomena and becomes relevant for many practical and technological applications, e.g. collective robotic motion, design and control of artificial microswimmers, and many other self-propelled particle systems[1–11] (see Ref. 12 for a recent review).

Within this broad context, the model early proposed by Vicsek *et al.*,[13] i.e. the so-called Vicsek Model (VM), has gained large popularity within the Statistical Physics community, which uses it as an archetypical model to study the onset of order upon the interactive displacement of self-driven individuals. The VM assumes that the individuals tend to align their direction of movement when they are placed within a certain interaction range. This rule, which would trivially lead to fully ordered collective motion, is complemented by a second one that introduces noise in the communications (interactions) among individuals. According to the Mermin–Wagner theorem, continuous symmetries cannot be spontaneously broken at finite temperature in equilibrium systems with short-range interactions in dimensions $D \leq 2$.[14,15] However, the nonequilibrium nature of the VM leads to a noise-driven phase transition even in two-dimensional ($2D$), which separates the ordered phase of collective motion (for noise amplitudes below the transition) from the disordered phase of noncollective motion (for noise amplitudes above the transition). Using a variety of approaches such as hydrodynamic equations,[16] long-range links in ad hoc complex network substrates,[17] and off-lattice simulations,[18] it has been shown that the particle displacements in the VM play the role of effective long-range interactions that are responsible for the onset of ordering.

In the original incarnation of the VM (specifically referred to as Standard VM (SVM)), fluctuations are implemented as *Angular Noise* (AN). Later, Grégoire and Chaté[19] proposed an alternative way of implementing fluctuations as *Vectorial Noise* (VN). These different implementations of noise are discussed in detail in Sec. 2. Intriguingly, it has been observed that the different kinds of flocking behavior (and even the nature of the phase transition as being discontinuous or continuous) could seem to depend on the way noise is implemented.[13,19–22] In the case of the VM with VN (VM-VN), the literature describes the transition as discontinuous (first-order).

In order to gain further insight into the VM dynamics and the onset of ordering, a complex network characterization of the structure of flocks in the SVM, i.e. the VM with AN (VM-AN), has recently been performed.[23,24] It was found that VM-AN flocks are essentially four-dimensional (4D) structures compactified into the $2D$ displacement space. It was also found that the topology of these flocks, once frozen (i.e. after disallowing further particle displacements, and evolving the system under a restricted SVM dynamics in which particles are only allowed to change orientation, similarly to spins in an XY-like model), are capable of sustaining ordered phases of

mean-field nature. Recalling that $D = 4$ is the upper-critical dimension of the XY model, and that, by virtue of the Mermin–Wagner theorem, XY-like equilibrium systems are prevented from exhibiting a phase transition in $2D$, those results were interpreted as confirming the effective $4D$ nature of VM-AN flocks.

Given the key role played by different kinds of noise implementation in the observed behavior of the VM, the aim of this paper is to follow up previous works[23,24] and investigate the topology of VM-VN flocks using standard tools from Complex Network theory. Besides performing an extensive complex network characterization of the structure of VM-VN flocks, we present a study of restricted VM-VN dynamics (where, as explained above, we allow only changes in orientation and treat particles as spins in an XY-like model defined on a "frozen flock substrate"). We analyze the results in the context of the theoretical implications of Mermin–Wagner and, whenever relevant, we compare our observations to those reported previously on the VM-AN case.

This manuscript is organized as follows: in Sec. 2, we define the model and the simulation method; Section 3 is devoted to the presentation and discussion of the results; finally, our conclusions are stated in Sec. 4.

2. The VM and the Simulation Method

The VM consists of a fixed number of interacting particles, N, which are moving on a $2D$ plane. The VM is perhaps the simplest model that captures the essence of collective motion in a nontrivial way. In computer simulations, the plane of motion is represented by a square with periodic boundary conditions. The particles move off-lattice with constant and common speed $v_0 \equiv |\mathbf{v}|$. Each particle interacts locally adopting the direction of motion of the subsystem of neighboring particles within an interaction circle of radius R_0, centered at the considered particle. The interaction radius is the same for all particles. Without loss of generality, we adopt the interaction radius as the unit of length throughout, i.e. $R_0 \equiv 1$. The average direction of motion of all particles within the interaction radius is perturbed by the presence of noise. There are two main variants of the model according to the way in which the noise is introduced: AN and VN.

The AN case was originally proposed by Vicsek *et al.*[13] and consists on the evaluation of the average angle of motion of the neighboring particles at time t, θ_j^t, which is then affected by a noise term. Hence, the updated direction of motion for the ith particle, θ_i^{t+1}, is given by

$$\theta_i^{t+1} = \mathrm{Arg}\left[\sum_{\langle i,j\rangle} e^{i\theta_j^t}\right] + \eta\xi_i^t, \tag{1}$$

where η is the noise amplitude, the summation is carried over all particles within the interaction circle centered at the ith particle, and ξ_i^t is a realization of a δ-correlated white noise uniformly distributed between $-\pi$ and π. The AN term can be thought of

as due to the error committed by the particle when trying to adjust its direction of motion to the averaged direction of motion of their neighbors. The VM-AN model has received much attention in the recent collective motion literature (see Ref. 12 and references therein). Although not the main focus of this work, we will repeatedly refer to previously reported VM-AN results as needed.

The VN was introduced by Grégoire and Chaté[19] as an alternative approach, in which noise arises from the interaction between the ith particle and each of its neighbors. So, instead of Eq. (1), the directions of motion are updated according to

$$\theta_i^{t+1} = \mathrm{Arg}\left[\sum_{\langle i,j\rangle} e^{i\theta_j^t} + \eta k_i e^{i\xi_i^t}\right], \tag{2}$$

where k_i is the number of neighbors of the ith particle.

In this paper, we implement the VM-VN model dynamics by adopting the so-called *backward update rule*: after the position and orientation of all particles are determined at time t, we update the position of the particles at time $t+1$ according to

$$\mathbf{x}_i{}^{t+1} = \mathbf{x}_i{}^t + \mathbf{v}_i{}^t \Delta t, \tag{3}$$

where $\Delta t \equiv 1$ is the unitary time-step. Equation (3) is then followed by the update of all velocities at time $t+1$ according to Eq. (1) or Eq. (2). For a detailed discussion on the impact of different updating rules, see Ref. 22.

The VM exhibits a far-from-equilibrium phase transition between ordered states of motion at low noise levels and disordered motion at high noise levels. This order–disorder transition is manifested by the natural order parameter of the system, namely the absolute value of the normalized mean velocity of the system, given by

$$\varphi = \frac{1}{Nv_0}\left|\sum_{i=1}^{N} \mathbf{v}_i\right|, \tag{4}$$

where φ is close to zero in the disordered phase and grows up to one in the ordered phase. The phase transition associated with the onset of large-scale ordered flocks in the VM-VN model is discontinuous (first-order).[19]

By definition, the VM is an automaton, i.e. all particles update their states simultaneously in one time-step. The particles move off-lattice in a $2D$ square of side $L = \sqrt{N/\rho}$, where ρ is the particle density. We adopt $v_0 = 0.5$ and $\rho = 2$ throughout. For these parameter values (which are standard in the literature), the system is known to undergo a first-order phase transition at the coexistence point $\eta_{\mathrm{coex}} = 0.613$.[25] Since we are interested in stationary configurations, we start out our simulations with random initial states and disregard the first 10^5 time-steps. We investigate different system sizes up to $N = 4 \times 10^5$. After reaching the stationary regime, we determine the set of connected clusters by means of the Hoshen–Kopelman algorithm[26] adapted for the case of off-lattice systems. In order to build a

set of complex networks that represent the stationary flocks generated by the VM-VN dynamics, we define that two individuals are linked if the distance between them is within the interaction radius R_0. Hence, complex networks representing flocks in the stationary regime are nonweighted and undirected.

From the perspective of our complex-network-based approach, the basic building blocks of the system are connected networks, where each node is an individual and a link represents a Vicsek-type interaction between individuals. For a given snapshot configuration of the system, the stationary state is statistically represented by a large ensemble of such connected networks (flocks). In order to improve the accuracy of our measurements, we generate 300 independent steady-state configurations, which are averaged to determine probability distribution functions of a number of statistical observables. In some instances, we also apply a moving average filter[27] to smooth out short-scale fluctuations from the probability distribution functions.

We also investigate the onset of orientation ordering in so-called *frozen clusters*. Clusters of individuals are first generated using the full VM-VN dynamics, as explained above. However, once the stationary flocks are obtained, the particle displacements (Eq. (3)) are suppressed. Within these frozen clusters, individuals are still allowed to change their orientation following the VN rule (Eq. (2)), with a noise amplitude in the range $0 < \eta_f < 1$, but their positions in the $2D$ displacement space remain fixed. Under this kind of restricted dynamics, the particle velocity vectors can be regarded as "spins" in an XY-like model defined on the complex network substrate provided by the flock topology.

3. Results and Discussion

Figure 1(a) shows a snapshot of a configuration in the stationary regime of the VM with VN (VM-VN), where $N = 4 \times 10^5$ individuals move in a $2D$ displacement space with periodic boundary conditions. It should be noticed that our implementation of the VM does not take into account volume exclusion effects due to the size of the particles, as considered in some recent versions of the model.[12] Some large-scale patterns (whose size is comparable to the dimensions of the box of particle displacements) are readily distinguishable in the snapshot of Fig. 1(a); however, micro- and mesoscopic patterns are much less discernible. As will be shown below, clusters are present in the system at all scales, from very small flocks formed by a few individuals to giant flocks that carry a sizeable fraction of the mass of the whole system.

Instead of focusing on patterns in the $2D$ displacement space, however, we will consider network representations of flocks of interacting particles following the definitions explained in Sec. 2. From this complex network interpretation, the length of the links does not correspond to the actual physical distance between neighbor particles, although the intrinsic modularization of the network structure carries significant spatial information. The advantage of the complex network perspective is that we can apply a well-developed conceptual framework, as well as a rich set of

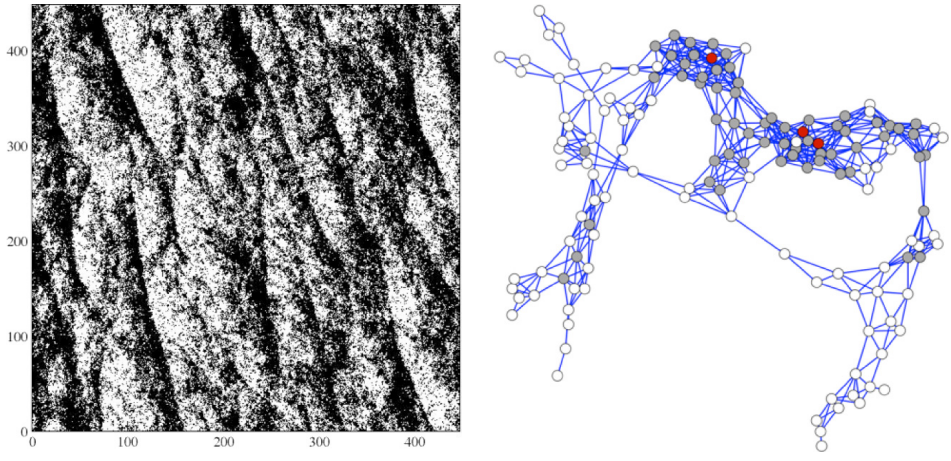

(a) (b)

Fig. 1. (Color online) (a) Snapshot of a VM-VN steady-state configuration with 4×10^5 individuals. (b) Representation of a VM-VN flock as a complex network with 148 nodes, 563 links and $\langle k \rangle = 7.6$. The color code of a node indicates its degree: white ($k/\langle k \rangle < 1$), gray ($1 \leq k/\langle k \rangle < 2$) and red ($2 \leq k/\langle k \rangle < 3$). The noise amplitude corresponding to both panels is $\eta = 0.56$ (below the coexistence point $\eta_{\text{coex}} = 0.613$).

computational tools, that enable us to fully characterize the system's topological properties.

Figure 1(b) shows the complex network structure of a typical VM-VN flock. Nodes are colored according to their degree: nodes with fewer connections than average ($k/\langle k \rangle < 1$) are shown in white, those slightly more connected than average ($1 \leq k/\langle k \rangle < 2$) in grey, and the highly connected ones ($2 \leq k/\langle k \rangle$) in red. Out of the 148 nodes (individuals) in this network (flock), we observe three highly connected ones that appear displayed in red. However, none of these nodes are network hubs that monopolize most of the links. In other words, the distribution of links is rather uniform, thus indicating the absence of leaders guiding the flock as a whole. There is an abundance of triangles, which indicates a high local clustering, whereas leaves (i.e. nodes with just one neighbor) are very uncommon. We also observe a pronounced modular structure with voids separating distinct modules within the flock, which suggests the lack of the small-world property.[28]

Stationary configurations are characterized by an ensemble of flocks of different sizes spanning many orders of magnitude. Figure 2 shows the probability distribution of cluster masses corresponding to different system sizes ($N = 4 \times 10^4$ and 4×10^5) as well as different noise values ($\eta = 0.30$ and 0.56). Notice that, here and throughout this paper, we define the mass of a connected cluster, m_c, as the number of its constituent nodes. Probability distribution functions (and moments thereof) are averaged over 300 independently generated steady-state configurations throughout. In Fig. 2, cluster mass distributions are power-laws with exponents in the range $1.6 \leq \beta_c \leq 2$, as indicated by the solid reference lines. Statistical errors are below 5%.

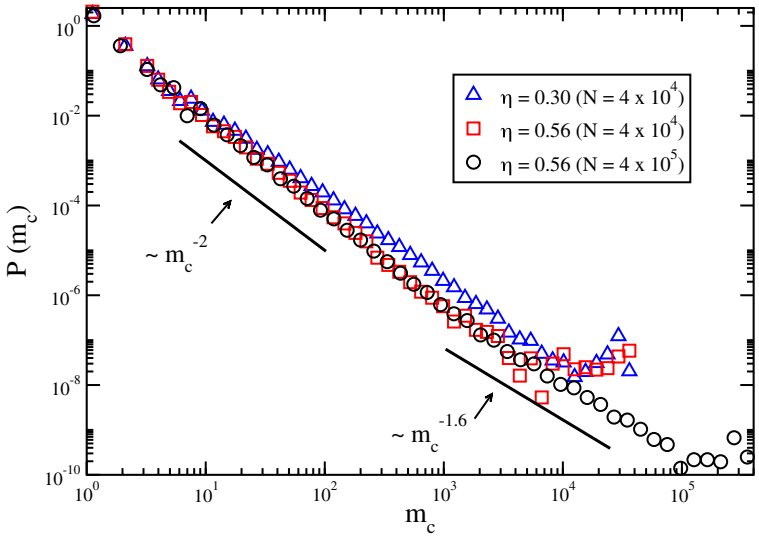

Fig. 2. (Color online) Cluster mass probability distributions for different levels of noise and system sizes, as indicated.

It is interesting to notice that, in the large-m_c region, the distributions depart from the power-law behavior, which suggests the existence of giant components, that is, very large clusters that carry a sizeable fraction of the mass of the entire system.

Let us now gain more insight into the structure of the clusters and evaluate the average path length (APL).[28,29] For each pair of nodes (A, B) within a connected cluster, the path length ℓ_{AB} (also known as chemical distance) is defined as the minimum number of links needed to get from node A to node B or vice versa (in undirected networks, this distance is the same in both directions). By calculating all pairwise node-to-node path lengths in the cluster and taking the average, one obtains the APL, which consequently is a characteristic length of the cluster.

Figure 3(a) shows a log–log plot of the APL as a function of the cluster size m_c. In Euclidean lattices, the volume of an object is related to its characteristic length by an integer power, i.e. the dimension of the object. Based on this observation, as well as on the experience gained in the study of fractal objects, it is customary to define the dimension (D) of a complex network according to:

$$\text{APL} \propto m_c^{1/D} \tag{5}$$

where m_c is the complex network size or, in the present context, the cluster mass.[29] The solid line in Fig. 3(a) shows the best fit of Eq. (5) to the data, which yields $D = 1.98(2)$, hence suggesting that VM-VN flocks are essentially 2D structures. It is interesting to point out that, in contrast to these findings, VM-AN flocks (i.e. flocks obtained using AN as prescribed by the so-called SVM) have an effective dimension $D = 4.0(2)$.[23,24] Notice that, here and throughout, error bars are determined from

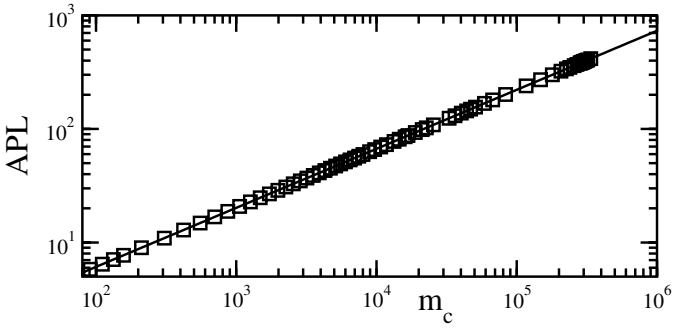

(a)

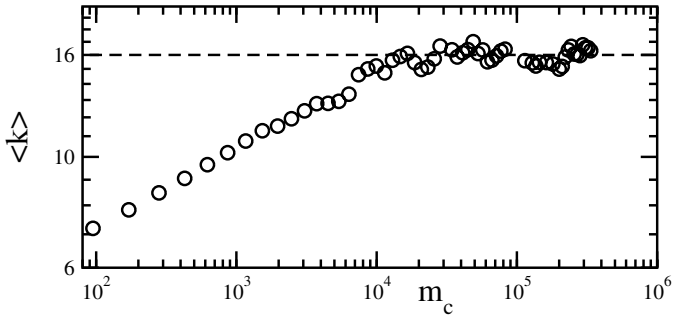

(b)

Fig. 3. (a) Log–log plot of the average path length APL as a function of the cluster size m_c. The fit of Eq. (5) to the data (solid line) yields $D = 1.98(2)$. (b) Log–log plot of the average degree $\langle k \rangle$ as a function of the cluster size m_c. The average degree saturates in the large cluster limit around the constant value $\langle k \rangle_s \approx 16$ (dashed line). In both plots, the noise amplitude is $\eta = 0.56$ (below the coexistence point $\eta_{\text{coex}} = 0.613$).

the fitting procedure, which takes into account the individual statistical error of each data point as well as its departure from the best-fitting function.

Figure 3(b) shows a log–log plot of the average degree $\langle k \rangle$ as a function of the cluster size m_c. The average degree of large clusters of mass $m_c > 10^4$ saturates around the constant value $\langle k \rangle_s \approx 16$. For clusters of mass $m_c < 10^4$, the mean degree is smaller than $\langle k \rangle_s$ due to a non-negligible surface-to-volume ratio of the spatial distribution of the flock mass (since surface nodes are less connected than bulk nodes). Interestingly, the average degree for VM-AN flocks scales with flock mass as a power-law, i.e. $\langle k \rangle \propto m_c^{\alpha}$, with $\alpha = 0.50(1)$, which has been shown to be consistent with VM-AN flocks being $4D$ structures compactified into the $2D$ displacement space.[23,24] In contrast, the results from Figs. 3(a) and 3(b) are consistent with VM-VN flocks being flat 2D objects with approximately constant coordination number (i.e. with similar topological properties as regular 2D lattices).

A very important topological measure of a complex network is the clustering coefficient, C.[28,29] The clustering coefficient for node i with k_i links is defined as

$$C_i = \frac{2n_i}{k_i(k_i-1)}, \tag{6}$$

where n_i is the number of links between the k_i neighbors of i. Then, the network's clustering coefficient is calculated as the average of C_i taken over all vertices, i.e. $C = \langle C_i \rangle$. Empirical results over a wide variety of real networks have shown that C is significantly higher for most real networks than for corresponding random networks of similar size.[28,30,31] Furthermore, the clustering coefficient of real networks is to a high degree independent of the number of nodes in the network.

Figure 4 shows the clustering coefficient C as a function of the cluster size m_c using the noise amplitude $\eta = 0.56$. Notice that flocks of all sizes display a very high degree of clustering, as we anticipated based on the high density of triangles observed in the network structure from Fig. 1(b). Also, we observe that the size dependence is very weak. By fitting the scaling relation $C \propto m_c^{-\gamma}$, we obtain $\gamma = 0.0017(1)$.

The asymptotic clustering coefficient in the limit of an infinitely large cluster, C_∞, has been shown to depend on the density of particles inside the cluster, ρ_{in}, according to

$$C_\infty = \frac{[(4\pi - 3\sqrt{3})\rho_{\text{in}} - 8]\pi\rho_{\text{in}}}{4(\pi\rho_{\text{in}} - 1)(\pi\rho_{\text{in}} - 2)}, \tag{7}$$

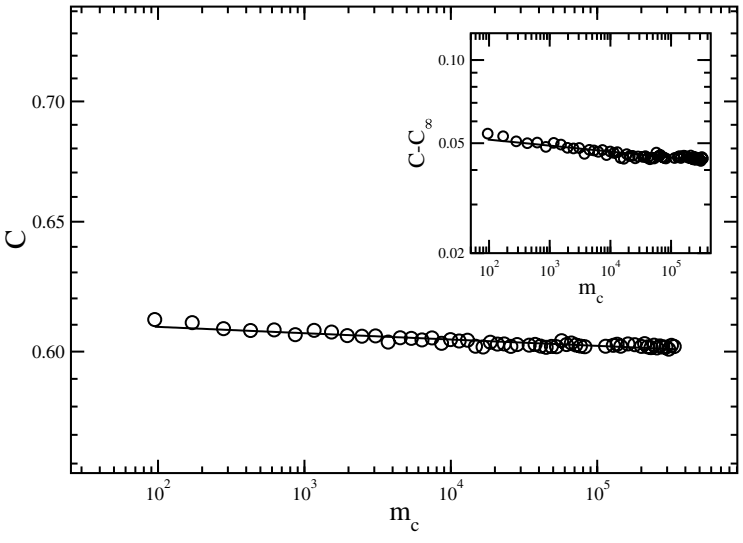

Fig. 4. Log–log plot of the clustering coefficient C as a function of the cluster size m_c. The solid line shows a power-law fit with exponent $\gamma = 0.0017(1)$. Inset: by subtracting the asymptotic clustering coefficient C_∞, the exponent $\gamma_\infty = 0.03(1)$ is determined.

which is expected to be an excellent approximation in the case of large clusters where the surface-to-bulk ratio is negligible.[24] Since we found that $\langle k \rangle_s \approx 16$ in the $m_c \to \infty$ limit, then Eq. (7) leads to $C_\infty \simeq 0.563$. The inset to Fig. 4 shows a log–log plot of $C - C_\infty$ as a function of the cluster mass m_c. The solid line shows a power-law fit for the decay of $C - C_\infty$ as a function of m_c, where the exponent is $\gamma_\infty = 0.03(1)$.

In order to determine whether modular organization is responsible for the high clustering coefficients seen in many real networks, Ravasz *et al.*[32,33] introduced the scaling law

$$C(k) \propto k^{-\beta_h}, \tag{8}$$

where $C(k)$ represents the distribution of the clustering coefficient as a function of the node degree and β_h is the exponent that measures the hierarchical structure of complex networks. Indeed, it has been observed that many real networks are composed of modules that combine into each other in a hierarchical manner. These hierarchical networks are uncovered by a scaling behavior of $C(k)$ that follows Eq. (8) with $\beta_h \simeq 1$. Figure 5 shows the log–log plot of $C(k)$ as a function of the degree. The drop with the degree is very mild, namely $\beta_h = 0.011(2)$, which points to a lack of hierarchical organization in the network structure of flocks. We argue that the emergence of a hierarchical topology is prevented due to the fact that links in the network construction process are distance-driven and limited by spatial constraints (since particles must lie within an interaction radius R_0 in order to be connected).

Another important network characterization is the degree of assortative mixing, i.e. whether high-degree vertices are preferentially attached to other high-degree vertices (in which case the network is termed assortative) or whether, on the

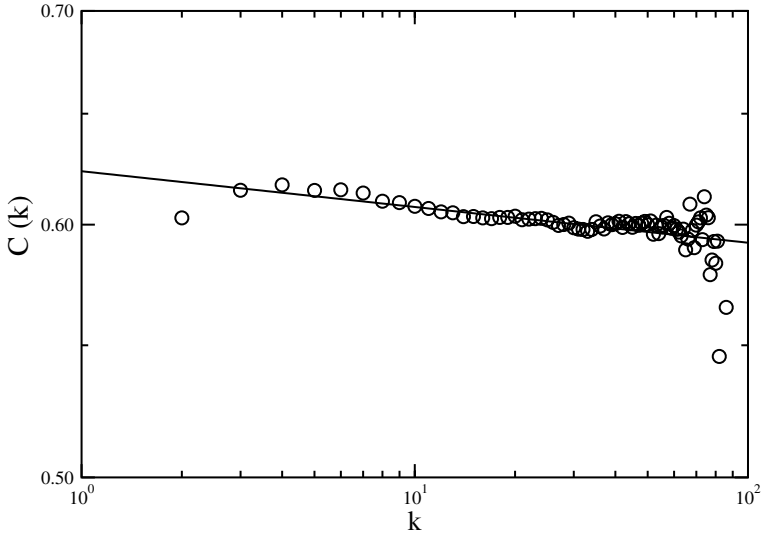

Fig. 5. Log–log plot of the clustering coefficient $C(k)$ as a function of the degree k, showing that the network topology of Vicsek flocks is nonhierarchical.

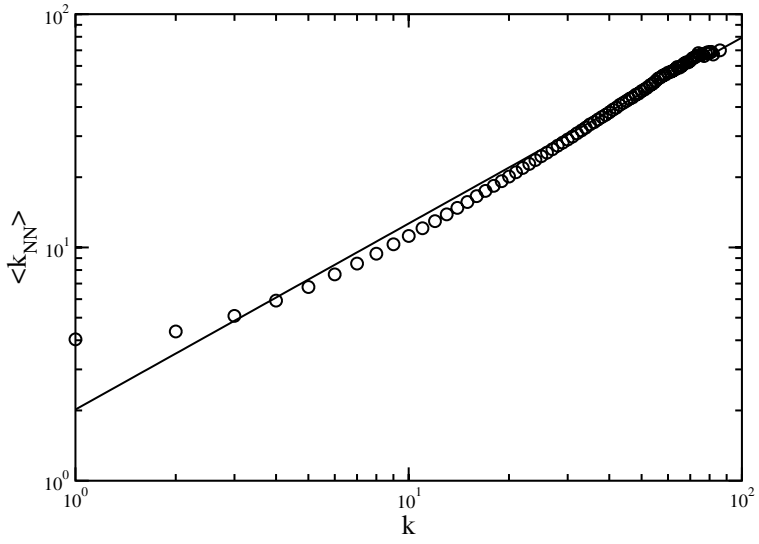

Fig. 6. Log–log distribution of the average degree $\langle k_{\rm NN}\rangle$ of nearest-neighbors of nodes of degree k. The solid line corresponds to a power-law fit with exponent $\gamma_a = 0.80(1)$, which reveals that VM-VN flocks are highly assortative.

contrary, high-degree vertices are preferentially attached to low-degree ones (in the case of disassortative networks).[34,35] Most often, social networks are assortatively mixed, while technological and biological networks tend to be disassortative. Network models such as classical random graphs and Barabási–Albert scale-free networks are neither assortative nor disassortative.

One way to determine the degree of assortative mixing is by considering the average degree $\langle k_{\rm NN}\rangle$ calculated among the nearest-neighbors of a node of degree k. Figure 6 shows the log–log plot of $\langle k_{\rm NN}\rangle$ as a function of k. The solid line shows the fit to a power-law $\langle k_{\rm NN}\rangle \propto k^{\gamma_a}$, where the assortativity exponent is $\gamma_a = 0.80(1)$, thus revealing a very high degree of assortative mixing. Alternatively, one can measure the degree of assortativity as the Pearson correlation coefficient of the degrees at either ends of an edge. This measure, originally introduced by Newman,[34] is obtained from the expression

$$r = \frac{1}{\sigma_q^2}\sum_{ij} ij(e_{ij} - q_i q_j), \tag{9}$$

where i, j are the degrees of the vertices at the ends of a given edge and the summation is carried over all edges in the network. Instead of using a node's degree k_i, here we are interested in the node's *remaining degree* $q_i = k_i - 1$ that excludes the edge between the two nodes being considered. Moreover, e_{ij} is the joint probability distribution of the remaining degrees of the two vertices at either end of a randomly chosen edge,[36] and $\sigma_q^2 = \sum_k k^2 q_k - [\sum_k k q_k]^2$ is the variance of the q_k distribution. The definition of r through Eq. (9) lies in the range $-1 \le r \le 1$, with assortative

networks having $r > 0$ and disassortative ones having $r < 0$. For instance, several scientific collaboration networks show assortative mixing in the range $0.12 \leq r \leq 0.36$, while the network of connections between autonomous systems on the Internet has $r = -0.19$ and the food web from undirected trophic relations in Little Rock Lake, Wisconsin has $r = -0.28$.[34] The Pearson correlation coefficient measured among large flocks turns out to be $r = 0.79(6)$, i.e. a very high assortative mixing.

As mentioned above, it is well-known that high local clustering and high assortativity are distinct hallmarks of social networks. Moreover, the imitation mechanism between neighboring interacting particles introduced by the VM dynamics resembles well-studied "ferromagnetic"-like interactions that play a key role in the occurrence of social cooperative phenomena.[37,38] Hence, these observed structural properties of VM flocks can be interpreted as arising from the social nature that underlies the behavior of individuals according to the VM dynamics.

As already discussed in Sec. 1, one of the most intriguing features of the VM is the onset of long-range ordering and the existence of a noise-driven order–disorder phase transition in $D = 2$ dimensions. In order to explore this phenomenon, here we analyze whether the topology of frozen clusters, once particle displacements and cluster rearrangements are suppressed, is capable by itself of supporting the ordered phase. For this purpose, we first generate configurations of clusters by applying the full VM-VN dynamics. Once the nonequilibrium stationary state is reached, we identify all connected clusters and "freeze" them, i.e. we disallow any further displacements of the individuals. From that point onwards, the orientation of the particles is allowed to evolve according to the rules for VN (Eq. (2)), but subsequent displacements (Eq. (3)) do not occur. We will refer to this stage as "restricted VM dynamics." Notice that the full VM dynamics has an entanglement between particle displacements and XY-type interactions. By resorting to "frozen clusters," we disentangle these two major components.

Figure 7 shows plots of φ versus m_c^{-1} for VM-VN frozen clusters. The clusters were first generated with $\eta = 0.56$ (below the first-order transition point at $\eta_{\text{coex}} = 0.613$) using the full VM dynamics, and after freezing them, different noise amplitudes η_f were used, as indicated. The extrapolations to the $m_c \to \infty$ limit are consistent with the absence of orientational ordering. The solid line is a power-law with exponent $1/2$, which is the expected behavior in the disordered phase according to the central limit theorem. Best fits to the data yield exponents equal to $0.52(2)$ (for $\eta_f = 0.7$) and $0.51(2)$ (for $\eta_f = 0.8$). Since the effective dimension of VM-VN clusters is $D = 2$, we can interpret the absence of the ordered phase by analogy with the XY model and the fact that, by virtue of the Mermin–Wagner theorem,[14,15] models having the same symmetries as the XY model cannot exhibit ordered phases in $D \leq 2$.

It is interesting to compare these results with an analogous frozen-cluster analysis of VM-AN flocks in the SVM.[23,24] In sharp contrast with the results from Fig. 7, it was then found that even for very large noise amplitudes, the order parameter in the large cluster limit ($m_c \to \infty$) tended to finite values, e.g. $\varphi \simeq 0.04$ for $\eta_f = 0.9$.

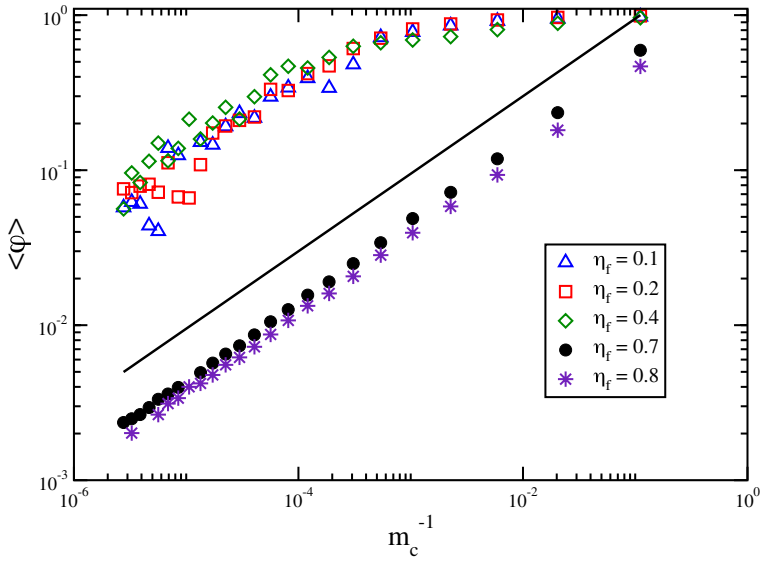

Fig. 7. (Color online) Log–log plot of the order parameter as a function of the inverse cluster mass for frozen clusters with different noise levels, as indicated. The solid line shows a power-law with exponent 1/2, which is the expected behavior in the disordered phase according to the central limit theorem.

Moreover, exact results from the mean-field solution obtained for an infinite density of individuals were found to closely follow the trend of the computer simulation results. How can these results be reconciled with Mermin–Wagner? The answer lies in the effective dimension of the complex network topology of VM flocks. In the VN case, the topology is that of the flat $2D$ structure of the displacement space. Therefore, the "frozen flock" structure is not able to sustain, by itself, XY-like ordered states; the existence of a VM-VN ordered phase relies therefore on the particle displacements at every time-step, which are introduced into the model dynamics via Eq. (3). In the AN case, instead, the complex network analysis showed that VM-AN flocks are $4D$ structures compactified into the two dimensions of the displacement space.[23,24] Thus, the VM-AN "frozen flock" topology is able to support XY-like ordered states; moreover, this ordered phase is of mean-field nature, as expected from the fact that $D = 4$ is the upper-critical dimension of the XY model.

4. Conclusions

In this paper, we presented a detailed study of the topological properties of VM flocks generated under VN. The complex network structure of VM-VN flocks is characterized by the absence of hubs (flock leaders), very high clustering, very high assortative mixing and nonhierarchical topology. Our findings are summarized in Table 1. These observations agree qualitatively with the structure of VM flocks generated under AN. We believe that these common features can be explained as due

Table 1. Summary of results for the topological analysis of VM-VN flocks.

Observable	Result
Cluster size distribution: $P \propto m_c^{-\beta_c}$	$\beta_c = 1.6 - 2$
Average path length: APL $\propto m_c^{1/D}$	$D = 1.98(2)$
Average degree distribution: $\langle k \rangle \propto m_c^{\alpha}$	$\alpha \approx 0$
Clustering coefficient distribution: $C \propto m_c^{-\gamma}$	$\gamma = 0.0017(1)$
Asymptotic clustering coefficient: C_∞	$C_\infty = 0.563$
Reduced clustering coefficient distribution: $C - C_\infty \propto m_c^{-\gamma_\infty}$	$\gamma_\infty = 0.03(1)$
Hierarchical modularity: $C(k) \propto k^{-\beta_h}$	$\beta_h = 0.011(2)$
Assortative mixing: $\langle k_{\mathrm{NN}} \rangle \propto k^{-\gamma_a}$	$\gamma_a = 0.80(1)$
Assortative mixing (Pearson correlation coefficient)	$r = 0.79(6)$
Frozen clusters: $\lim_{m_c \to \infty} \varphi$	No Ordering

to the intrinsic distance-driven, "ferromagnetic" nature of the VM. Indeed, the model's geographical constraints cause the flocks to lack hubs or any modular hierarchies, while the alignment dynamics explain the very high local clustering and assortative mixing, resembling the typical topology of social networks. Based on this evidence, we describe VM flocks as geographically-constrained "social" networks.

In order to gain further insight into the onset of order in the VM, we disentangled the two main ingredients of the model dynamics, namely particle displacements and particle alignments (i.e. rotations of the velocity vectors). By resorting to "frozen clusters" in a restricted VM dynamics, we found that the topology of VM-VN flocks is incapable of supporting orientation ordering of the resulting XY-like model, which agrees with the expectations from the Mermin–Wagner theorem for $2D$ equilibrium systems. However, these findings are in sharp contrast with VM-AN frozen flocks, which are indeed capable of sustaining ordered states in the thermodynamic limit, as shown in Refs. 23 and 24. The apparent paradox is resolved when the effective dimension of VM-AN flocks is taken into account: the topology of VM-AN flocks is $4D$, and therefore the restricted dynamics leads to mean-field like ordered states, in agreement with the expected behavior of $4D$ XY-like models.

The main goal of this paper was to complement previous work in order to analyze Vicsek Model flocks from a topological perspective, thus underlining relevant similarities and differences arising from different (and widely studied) implementations of noise in the model. Certainly, further efforts are needed to understand the interplay between model dynamics and structure, as well as the intriguing onset of order under different conditions. We hope that this work will stimulate further investigations in the complex yet fascinating field of cooperative phenomena in self-propelled particle systems.

Acknowledgments

We are very grateful to F. Vázquez for fruitful discussions. This work was financially supported by CONICET, UNLP and ANPCyT (Argentina).

References

1. J. L. Deneubourg and S. Goss, *Ethol. Ecol. Evol.* **1**, 295 (1989).
2. E. V. Albano, *Phys. Rev. Lett.* **77**, 2129 (1996).
3. A. Czirók, E. Ben-Jacob, I. Cohen and T. Vicsek, *Phys. Rev. E* **54**, 17911801 (1996).
4. E. Bonabeau, L. Dagorn and P. Fréon, *J. Phys. A: Math. Gen.* **31**, L731 (1998).
5. W. J. Rappel, A. Nicol, A. Sarkissian, H. Levine and W. F. Loomis, *Phys. Rev. Lett.* **83**, 1247 (1999).
6. X. L. Wu and A. Libchaber, *Phys. Rev. Lett.* **84**, 3017 (2000).
7. G. Theraulaz, E. Bonabeau, S. C. Nicholis, R. V. Sole, V. Fourcassié, S. Blanco, R. Fournier, J. L. Joly, P. Fernández, A. Grimal, P. Dalle and J. L. Deneubourg, *Proc. Nat. Acad. Sci.* **99**, 9645 (2002).
8. K. Sugawara and T. Watanabe, *Proc. FIRA Robot World Congress* **5**, 3214 (2002).
9. C. Becco, N. Vandewalle, J. Delcourt and P. Poncin, *Physica A* **367**, 48793 (2006).
10. T. Feder, *Phys. Today* **60**, 28 (2007).
11. G. Baglietto and D. R. Parisi, *Phys. Rev. E* **83**, 056117 (2011).
12. T. Vicsek and A. Zafeiris, *Phys. Rep.* **517**, 71 (2012).
13. T. Vicsek, A. Czirók, E. Ben-Jacob and O. Shochet, *Phys. Rev. Lett.* **75**, 1226 (1995).
14. N. D. Mermin and H. Wagner, *Phys. Rev. Lett.* **17**, 1133 (1966).
15. N. D. Mermin, *J. Math. Phys.* **8**, 1061 (1967).
16. J. Toner and Y. Tu, *Phys. Rev. Lett.* **75**, 4326 (1995).
17. M. Aldana, V. Dossetti, C. Huepe, V. M. Kenkre and H. Larralde, *Phys. Rev. Lett.* **98**, 095702 (2007).
18. G. Baglietto and E. V. Albano, *Comput. Phys. Commun.* **180**, 527 (2009).
19. G. Grégoire and H. Chaté, *Phys. Rev. Lett.* **92**, 025702 (2004).
20. M. Nagy, I. Daruka and T. Vicsek, *Physica A* **373**, 445 (2007).
21. M. Aldana, H. Larralde and B. Vázquez, *Int. J. Mod. Phys. B* **23**, 3661 (2009).
22. G. Baglietto and E. V. Albano, *Phys. Rev. E* **80**, 050103(R) (2009).
23. G. Baglietto, E. V. Albano and J. Candia, *Interface Focus* **2**, 708 (2012).
24. G. Baglietto, E. V. Albano and J. Candia, *J. Stat. Phys.* **153**, 270 (2013).
25. G. Baglietto and E. V. Albano, *Int. J. Mod. Phys. C* **17**, 395 (2006).
26. J. Hoshen and R. Kopelman, *Phys. Rev. B* **14**, 3438 (1976).
27. N. J. Saldkind (ed.), *Encyclopedia of Measurements and Statistics* (Sage Publications, Thousand Oaks, London, New Delhi, 2007).
28. R. Albert and A.-L. Barabási, *Rev. Mod. Phys.* **74**, 47 (2002).
29. S. N. Dorogovtsev, A. V. Goltsev and J. F. F. Mendes, *Rev. Mod. Phys.* **80**, 1275 (2008).
30. D. J. Watts and S. H. Strogatz, *Nature (London)* **393**, 440 (1998).
31. S. N. Dorogovtsev and J. F. F. Mendes, *Adv. Phys.* **51**, 1079 (2002).
32. E. Ravasz, A. L. Somera, D. A. Mongru, Z. N. Oltvai and A.-L. Barabási, *Science* **297**, 1551 (2002).
33. E. Ravasz and A.-L. Barabási, *Phys. Rev. E* **67**, 026112 (2003).
34. M. E. J. Newman, *Phys. Rev. Lett.* **89**, 208701 (2002).
35. M. E. J. Newman, *Phys. Rev. E* **67**, 026126 (2003).
36. D. S. Callaway, J. E. Hopcroft, J. M. Kleinberg, M. E. J. Newman and S. H. Strogatz, *Phys. Rev. E* **64**, 041902 (2001).
37. C. M. Bordogna and E. V. Albano, *Phys. Rev. Lett.* **87**, 118701 (2001).
38. J. Candia, *J. Stat. Mech.* P09001 (2007).